Solid Earth Discuss., 7, 1263–1314, 2015
www.solid-earth-discuss.net/7/1263/2015/
doi:10.5194/sed-7-1263-2015

Solid Earth Discussions
Open Access

Jurassic–cretaceous deformational phases in the Paraná intracratonic basin, southern Brazil

A. J. Strieder[1,*], R. Heemann[2], P. A. R. Reginato[3], R. B. Acauan[4], V. A. de Amorim[5], and M. Z. Remde[6]

[1]Engenharia Geológica, Centro de Engenharia, UFPel Praça Domingos Rodrigues 02, Bairro Porto, Pelotas-RS, Brazil
[2]PUC-RS, Porto Alegre-RS, Brazil
[3]IPH, UFRGS, Porto Alegre-RS, Brazil
[4]FEPAM, Porto Alegre-RS, Brazil
[5]Geologist, Professional Services, Brazil
[6]Engineering Geologist, Professional Services, Brazil
[*]now at: CERENA – Centro de Recursos Naturais e Ambiente Instituto Superior Técnico (Universidade de Lisboa), Av. Rovisco Pais Lisboa 1049-001, Portugal

Received: 11 March 2015 – Accepted: 11 March 2015 – Published: 2 April 2015

Correspondence to: A. J. Strieder (adelirstrieder@uol.com.br)

Published by Copernicus Publications on behalf of the European Geosciences Union.

Abstract

This paper examines the domes and basins, regional arcs and synclines, and brittle structures of the Paraná Basin flood volcanism to characterize the deformational phases in its Jurassic to Cretaceous history. First-stage fieldwork revealed brittle structures, extensional joints, and strike-slip faults, and second-stage fieldwork investigated the connections of the brittle structures to both open folds and dome-and-basin features. Fault-slip data inversion was performed using two different techniques to distinguish local and remote stress/strain. Geometric and kinematic analyses completed the investigations of the deformation, which characterized two deformational phases for the Jurassic to Cretaceous periods in the Paraná Basin. Both developed under regional bi-directional constrictional ($\sigma_1 \geq \sigma_2 \gg \sigma_3$) stress regimes that produced a number of non-cylindrical folds. A D1 deformational phase produced the N–S and E–W orthogonally oriented domes and basins. The D2 arcs and synclines are oriented towards the NW and NE and indicate a clockwise rotation (35–40°) of both horizontal principal stress tensors. The extensional joints and strike-slip faults characterize the local stress field in the outer rim of the orthogonally buckled single volcanic flow, whereas the inner rim of the buckled single flow supported constriction and thus, developed the local arcuate folds.

1 Introduction

The Paraná Basin is located in the South America Plate (Fig. 1) and is characterized as a huge Paleozoic to Mesozoic intracratonic depression filled by sedimentary and volcanic rocks (see Zalán et al., 1991; Zalán, 2004). The regional stratigraphic correlation and facies change for the uppermost sequences in the Paraná Basin (São Bento Group) remain controversial, since Scherer and Lavina (2006) correlated the Piramboia Fm. with Neo-Permian sedimentary units, while Soares et al. (2008a) correlated it with Neo-Triassic to Jurassic sedimentary units. The regional isopach maps for the

Mesozoic sedimentary sequence (Artur and Soares, 2002; Soares et al., 2008b) fit well with the results presented here. Thus, the proposition by Soares et al. (2008a) is adopted to characterize the Jurassic–Cretaceous stratigraphic interval of the Paraná Basin. As a result, the São Bento Group is considered to comprise the Pirambóia and Guará (Eo to Meso-Jurassic), Botucatu (Neo-Jurassic), and Serra Geral (Cretaceous) formations (Soares et al., 2008a). The Serra Geral Formation is mainly composed of volcanic rocks, well known as the Paraná–Etendeka Flood Basalt Province (Wilson, 1989).

The main structural features of the Paraná Basin were recognized using satellite imagery lineaments and fault plane trends (e.g., Soares et al., 1982; Zerfass et al., 2005; Reginato and Strieder, 2006; Strugale et al., 2007; Machado et al., 2012; Nummer et al., 2014; Jacques et al., 2014), geophysical lineaments (e.g., Ferreira, 1982; Ferreira et al., 1989; Quintas, 1995), or isopach maps developed for each sedimentary sequence (e.g., Northfleet et al., 1969; Artur and Soares, 2002). The main findings include regional lineaments, arcs, and flexures (Fig. 1) that have been summarized by Almeida (1981), Zalán et al. (1991), and Zalán (2004). These authors also highlighted the influence of the basement on the development of these structural features in the Paraná Basin. These regional-scale structural features deform the entire Paraná Basin sequence and do not depend on the stratigraphic interpretation of the uppermost sequences.

Riccomini (1995) conducted the first paleostress investigation of the uppermost stratigraphic units of the Paraná Basin, and distinguished a number of deformational phases from the Permian units of the Paraná Basin through to the Holocene continental margin rift basins (Table 1) by applying the method of Angelier and Mechler (1977). The main criterion used to distinguish the deformational phases was to separate fracture direction families. Riccomini (1995) interpreted these deformational phases by considering transcurrent regimes, mainly due to the large predominance of striae parallel to the fault strike and based on propositions suggesting differential movements dur-

ing South American and African plate rotation after Gondwana rifting (Morgan, 1983; Chang et al., 1992; Riccomini, 1995).

Recently, Strugale et al. (2007) distinguished two deformational phases in the Jurassic and Cretaceous of the Ponta Grossa Arc region. These deformational phases can be correlated to D_{n+1} and D_{n+2} described by Riccomini (1995). Similarly, Machado et al. (2012) and Nummer et al. (2014) distinguished three deformational phases in the high hills of the Torres Syncline. These phases can also be correlated with the D_n, D_{n+1}, and D_{n+2} phases proposed by Riccomini (1995).

Heemann (1997, 2005), Reginato (2003), Acauan (2007), and Amorim (2007) also applied the Angelier and Mechler (1977) method to fault slip data from volcanics and interlayered aeolian sandstones of the Serra Geral Fm. However, their work, which involved a geometric and symmetry analysis of fault slip data, enabled deformational phases to be distinguished. Consequently, Heemann (1997, 2005), Reginato (2003), Acauan (2007), and Amorim (2007) distinguished two deformational phases: (i) a NS and EW oriented stress field, and (ii) a NW and NE oriented stress field; however, they could not determine which of these was the first. Strieder and Heemann (1999) and Reginato and Strieder (2006) highlighted the NS–EW orthogonal pattern of the sandstone dikes and mineralized veins emplaced into the basalts. Heemann (1997, 2005), Reginato (2003), Acauan (2007), and Amorim (2007) also identified areas with opposite positioning of the maximum and minimum stress axes (Table 2), although their findings were difficult to interpret. Therefore, these results need to be investigated further using additional fault slip data and fault geometry analysis.

The present study aimed to report the results of a large-scale structural analysis survey conducted within the Serra Geral and the underlying Botucatu formations. An analysis of the brittle structures focused mainly on stress inversion techniques applied to fault-slip data from volcanic rocks in order to distinguish the different phases of deformation and evaluate the paleostress field during the Jurassic to Cretaceous periods.

The paper presents a geometrical and kinematical analysis of mesoscale faults (10–100 m long) studied at 42 sites (quarries and large road cuts) located within the central

region and eastern border of the Paraná Basin. To constrain their times of occurrence, a number of local and regional structural elements were used to characterize these deformational phases: fault plane, slip direction and sense, type of kinematic indicator, fault splay geometry, fracture opening and infilling, large-scale folding and dome-and-basin features, and the basal contact of the Botucatu and Serra Geral formations.

The paper discusses the tectonic conditions within which the paleostress axis inversion operated and the orthogonal joint pattern developed. Orthogonal joint formation and its associated stress inversion remain subjects of discussion, and a number of mechanisms have been proposed to account for the local and regional deformational features (see Caputo, 1995; Caputo and Hancock, 1999; Bai et al., 2002). Based on these elements, the mesoscale fault geometries and fault-slip data of the rocks of the Serra Geral Fm. have been shown to be reliable indicators of the distribution of the local paleostress state in the Paraná Basin during the Jurassic to Cretaceous periods.

2 Fieldwork and structural analysis methods

The regularities of the preliminary paleostress fields recorded in the volcanic rocks of the Serra Geral Fm. at different sites inspired a second stage of fieldwork, which involved both revisiting previous sites to obtain a more complete structural study and surveying new sites in the southern Paraná Basin.

A third stage of fieldwork was performed to characterize the gentle folds and dome-and-basin structures developed within the Botucatu and Serra Geral formations. The procedure for characterizing such structures involved their identification from satellite imagery or aerial photographs, followed by fieldwork to measure the sandstone–basalt contact orientations, or the basal surface of a given basalt flow.

2.1 Fieldwork methods for brittle structures

The structural geology studies were undertaken in open-pit quarries, underground openings, and large road cuts. The investigation of the brittle structures from the 42 sites involved analysis of the slip direction and sense of movement of more than 800 fault planes. To ensure the confidence of the results, only those records with a clearly defined slip sense were sampled for the computation of the paleostress fields.

Field investigations also included geometrical data records based on fracture splaying (Fig. 2). Fracture splaying shows patterns similar to synthetic fractures developed during shear experiments (e.g., Tchalenko, 1970; Tchalenko and Ambraseys, 1970). Most fracture patterns exhibit open spaces and at least one of those fractures is mineralized. Mineralization is composed of carbonate, chalcedony, and zeolites, or a combination of carbonate + chalcedony + celadonite. The fracture patterns and mineralization of dilatational spaces can be observed on different scales, but their geometric relationships are more easily distinguished on the outcrop scale. A field diagram was developed to compile and record different fracture patterns (Fig. 3).

Kinematic indicators include a variety of types, but frictional steps and the accretionary growth of crystal fibers (Hancock, 1985), and RM and TM types of secondary fracture steps (Petit, 1987) largely predominate (Fig. 4). Some fault planes display different slip striations and movements, and occasionally crosscutting (truncation) relations could be recorded (Fig. 4b). The truncation between different striations in the same plane suggests their age relation (Table 3). A rare melted and polished fault plane with slip striae is shown in Fig. 4c and ductile drag deformation of the horizontal joints can be observed in Fig. 4d in the basaltic rock with the development of a fracture cleavage.

2.2 Methods for evaluation of deformational phases in the Serra Geral Fm.

The first approximations for paleostress regimes in the volcanic rocks of the Paraná Basin used the graphical method described by Angelier and Mechler (1977). This

graphical method superposes *P* and *T* dihedrals for each element of fault-slip data, which allows paleostress regimes to be distinguished by grouping compatible fracture splay geometries and fault slip data.

In the second phase of the paleostress analysis, the above graphical method was combined with a numerical stress-inversion technique (Žalohar and Vrabec, 2007, 2008). The separation of paleostress regimes from heterogeneous fault systems is tedious. In the present case, the complete fault-slip data sets were tested by applying the Gauss method described by Žalohar and Vrabec (2007). This method defines a Gaussian compatibility function based on the adjustment measure between the angular misfit and the normal to the shear stress ratio on the fault plane. The Gauss method proposed by Žalohar and Vrabec (2007) can distinguish between heterogeneous fault-slip data, as is the present case. Then, the Gauss method was applied site-by-site to limit the fault-slip data numbers and to evaluate local heterogeneities in the paleostress regimes of the Paraná Basin volcanic rocks. In order to obtain numerically stable results, the fault-slip data of some sites were merged based on their proximity, fault-slip consistency, geometry, and fault pattern. The merged fault-slip data represent small areas of the Paraná Basin under homogeneous stress/strain conditions. These fault-slip data were then reprocessed and the results used for the structural analysis discussion.

The stress inversion was performed using the T-TECTO 3.0 program (http://www2.arnes.si/~jzaloh/t-tecto_homepage.htm) developed by Dr. Jure Žalohar. The paleostress/paleostrain regimes were determined using the Gauss method and kinematic multiple-slip method (MSM) (Žalohar and Vrabec, 2008). The MSM calculates weighting factors for moment tensor summation based on the number and orientation of parallel faults of the same size range, direction of slip along them, and the mean rock properties. The parameters for stress inversion by MSM are shown in Table 4.

The reduced tensors calculated by these methods can be interpreted either as the stress or strain tensor. The Gauss method is an inverse-method that is applied to define paleostress (Žalohar and Vrabec, 2007), whereas the MSM is used as the direct kinematic paleostrain method (Žalohar and Vrabec, 2008).

3 Regional structural features in the Jurassic–Cretaceous units of the Paraná Basin

Figure 1 shows some structural features that affect the stratigraphic units of the entire Paraná Basin; however, some are of particular interest with regard to the Jurassic–Cretaceous interval because it will be shown here that they were developed during the deformational phases.

The most prominent structures are the large-scale anticlinal and synclinal gentle folds in the eastern border of the Paraná Basin (Fig. 5), which show NW-dipping hinges (see Zalán et al., 1991). Erosion of the anticlines created the area in which the volcanic and sedimentary rocks of the Paraná Basin are exposed towards the NW, and gave rise to the Rio Grande and Ponta Grossa arcs. However, the folds are not cylindrical, but produce elliptical domes and basins (details in Fig. 5).

The presence of large domes in the Serra Geral volcanics has long been reported (e.g., Lisboa and Schuck, 1987; Schuck and Lisboa, 1988; Rostirolla et al., 2000). Similar structures were also described for underlying sedimentary sequences (Riccomini, 1995). Close examination of these structural features reveals that they are an association of gentle domes and basins, which can be classified into two groups: (a) those with N–S or E–W orientation, and (b) those with NW or NE orientation. Some examples of such domes are indicated in Fig. 5: (a) Quaraí Dome, (b) Rivera Crystalline Island, and (c) Aceguá Crystalline Island. The longest axis of these domes is < 100 km. The Quaraí Dome shows a NE orientation of its longest axis, while the Rivera and Aceguá crystalline islands exhibit EW orientation. Aboy and Masquellin (2013) presented some structural and sedimentary evidence supporting the uplift of the Rivera Crystalline Island from the Permian period onwards.

The basal contact of the Serra Geral Fm. volcanic rocks was measured in a number of outcrops to constrain the deformation related to the NW-dipping anticlines–synclines (Fig. 5a). Figure 5b shows that the axes of these continental-scale gentle folds are oriented towards 06/308. A balanced SW–NE structural section (Fig. 6) illustrates the

relationships between the anticlines–synclines from Uruguay to São Paulo (Brazil). This regional cross section was balanced as concentric folds (Marshak and Mitra, 1988; pp. 269–302).

Structural mapping was conducted in the Quaraí Dome area, close to the Brazil–Uruguay border (Fig. 7a). In this area, the erosion of volcanic flows over the Botucatu Fm. sandstones allows a number of domes and basins with different orientations to be recognized. The most important of these is the Quaraí Dome, because it has the greatest amplitude and it exposes the underlying Botucatu Fm. sandstone. Measurements of the sandstone–basalt contact show that the Quaraí Dome is oriented towards 02/043 (Fig. 7b).

North and northwest of the Quaraí Dome, two elongated basins (N–S and E–W, respectively) can be recognized (Fig. 7a). The attitudes of the thin volcanic flows are shown for the E–W-dipping (Fig. 7c) and N–S-dipping (Fig. 7d) long axes for both basins.

The N–S-oriented folds were also recognized on the outcrop scale (Fig. 7e). This fold is developed upon the Botucatu Fm. sandstone and it was identified in the inner part of the Quaraí Dome along the BR-293 road. The eolian stratification was deformed around an 11/176 folding axis (Fig. 7f).

The map in Fig. 7a shows that the domes and basins with the same orientation do not interfere with each other. The folds are described as non-cylindrical and arcuate in map view. The fold tightness varies from gentle (interlimb angle: 170° for small domes and basins, 151° for the Quaraí Dome, and 159° for regional arcs) to open fold (interlimb angle: 120° for the N–S outcrop fold).

4 Paleostress tensors in the Serra Geral Fm. volcanic rocks

The results of the fault-slip data processing are presented in a sequence of figures for each site/area (Figs. 8 and 9). The figures include the Wulff projection (lower hemisphere) of the brittle fault-slip data, misfit angle histogram, unscaled Mohr diagram for

resolved stress on the faults, and a diagram relating the values for the object function (M) and shape of the strain ellipsoid (D). The object function depends on the parameters defined in Table 4, and relates the SD (s) of angular misfit between the direction of slip along the faults (striae) and the shear stress produced by a given tensor. Therefore, its value is used to determine the best orientation of stress tensor for those fault-slip data (Žalohar and Vrabec, 2007).

The structural analysis performed on the Serra Geral Fm. volcanic rocks (Paraná Basin) distinguished two different paleostress fields:

a. Predominantly N–S-oriented maximum horizontal stress with permutations to the E–W;

b. predominantly NE–SW-oriented maximum horizontal stress with permutations to the NW–SE.

In both cases, the intermediate principal stress (σ_2) is subvertical, which explains the prevalence of strike-slip faulting. The crosscutting relations between striations (Table 1) indicate that the N–S maximum horizontal stress is older than the NE–SW stress. This interpretation is also consistent with other structural features such as the elliptical domes.

These general orientations for the NE–SW (NW–SE) stress tensors agree with those presented by Riccomini (1995), Strugale et al. (2007), Machado et al. (2012), and Nummer et al. (2014). They differ, however, on processing methodology and kinematic analysis. It should be noted that the area studied by Riccomini (1995) and Strugale et al. (2007) is heavily influenced by the NW–SE Ponta Grossa faults and dikes. Despite final results that are difficult to reconcile, it seems that the D1 faults (deformation) defined by Strugale et al. (2007) correspond to the D2 deformational phase discussed here.

4.1 Predominantly N–S-oriented maximum horizontal stress with permutations to the E–W

The maximum (σ_1) and minimum (σ_3) compressive paleostresses are subhorizontal (Fig. 8). These main paleostress axes are oriented close to the N–S and E–W directions and in most cases, the stress ratio (Φ) ranges from 0.10–0.30. The mean misfit angle of the fault-slip data for each site/area is < 15° (see Fig. 8), while the SD is < 20° (see Table 5). These conditions suggest a strike-slip regime and the observed fault-slip data indicate the presence of conjugate patterns of faults (Fig. 8).

This group of tensors shows the permutations of the maximum (σ_1) and minimum (σ_3) compressive paleostress axes between the N–S and E–W directions. In Fig. 8a, b, e, and g, the maximum compressive (σ_1) paleostress axis is close to the E–W direction, whereas in Fig. 8c, d, f, h, and i, the maximum compressive (σ_1) tensor is close to the N–S direction. Such results, recorded in the CODECA quarry (Fig. 6g and h), were initially intriguing and demanded a careful re-investigation of the fault-slip at this site. The alternated orientation of the maximum paleostress axis was observed at other sites/areas within the Paraná Basin volcanic rocks. Furthermore, the alternation of the stress tensor occurs in some tectonic regimes (Angelier, 1989) and this aspect will be considered later.

4.2 NE–SW maximum horizontal compression

This group of paleostress tensors is also related to the subhorizontal maximum and minimum compressive stresses, while the intermediate stress axis (σ_2) is subvertical (Fig. 9). The maximum horizontal compressive stress is oriented close to NE–SW and the stress ratio (Φ) ranges from 0.10–0.30. These conditions also suggest a strike-slip stress regime and the presence of a conjugate pattern of faults (Fig. 9).

The mean misfit angle of the fault-slip data for each site/area is close to 15° (see Fig. 7) and the SD is < 18° (see Table 6). Table 6 summarizes the results of the stress inversion for this fault-slip data set.

The paleostress tensors also indicate the permutations between the maximum (σ_1) and minimum (σ_3) compressive stress axes from the NE–SW to NW–SE directions in some sites/areas (Santa Rita quarry) (see Fig. 9a–f).

5 Geometric and kinematic analyses of deformational structures in the volcanic rocks

The regional-scale folds (Fig. 5) and the domes and basins (Fig. 7) discussed in the previous sections show systematic relationships with the fracture patterns (Figs. 8 and 9). Thus, the deformational structures developed within the volcanic rocks of the Serra Geral Fm. are analyzed considering the fracture patterns.

The geometric and kinematic analyses of fracture patterns use rose diagrams to classify conjugated and splay fractures observed in each site/area, because the strike-slip stress regime developed subvertical to vertical fractures. This procedure makes it possible to distinguish the synthetic and antithetic fractures and to determine the mean ϕ (internal friction angle; see Jaeger, 1969; Angelier, 1989).

5.1 Fracture patterns of N–S paleostress tensors

The fracture patterns developed in the N–S maximum horizontal compression clearly indicate conjugate geometry, as can be seen in Fig. 10. However, it is clear that dextral and sinistral conjugate sets show different spatial distributions (orientations) and frequency.

The rose diagrams in Fig. 10 show fracture orientations according to the synthetic Riedel fracture criteria (Tchalenko, 1970) and reinforce the field observations (Fig. 2). The rose diagrams indicate the predominance of R-type fractures and some diagrams illustrate the presence of fractures at angles lower than 15–20° relative to the main compressive stress axis (σ_1). These fractures are classified as hybrid joints (Hancock, 1985).

R-type fractures usually merge with C-type fractures to develop splay or duplex fracture patterns, and hydraulic breccia are often associated with such dilatational spaces. The dilatational space is filled by a zeolite ± quartz ± chalcedony ± calcite ± celadonite paragenesis.

The geometric and kinematic analyses of the N–S-directed paleostress field also consider the occurrence of tabular dykes of thermally metamorphosed sandstone emplaced into the vesicular basalts (Fig. 11a) of the Serra Geral Fm. sequence. A detailed field survey of their orientation was undertaken in the Salto do Jacuí region. Figure 11b shows that these tabular dykes are predominantly subparallel to the maximum compressive stress axis (σ_1) when it is oriented either to the N–S or to the E–W.

In the Caxias do Sul region, the thermally metamorphosed sandstone tabular dykes were measured cutting across the massive basalts of the Serra Geral Fm. Figure 11c shows that such dykes are also oriented to the NE–SW; however, they still show the main distribution in the N–S and E–W directions. In the Caxias do Sul region, a large number of mineralized veins were measured. Figure 11d shows that opened fractures are mainly oriented in the N–S, E–W, and NW–SE directions.

The orientation of metamorphosed sandstone dykes in the Salto do Jacui and Caxias do Sul regions are slightly different. For the Salto do Jacui region, the preferred orientation is N10E, whereas in the Caxias do Sul region, it is N10W. However, such differences are in accordance with the local stress field orientations, as can be seen in Fig. 8c, d, e, g, and h.

The sandstone dykes and mineralized veins cutting across the basalts are controlled by an orthogonal pattern of fractures. This observation agrees with the permutations of the maximum (σ_1) and minimum (σ_3) compressive paleostress axes between the N–S and E–W directions, as reported above.

This orthogonal pattern (N–S and E–W) is also observed in the Cerro do Jarau giant intertrap dune (Remde, 2013). The orthogonal pattern in the Cerro do Jarau area (Fig. 7a), however, is defined by centimeter-scale veins in the basalts (Fig. 12a), and mainly by millimeter-scale deformation bands in the intertrap Botucatu Fm. sandstone

(Fig. 12b). The centimeter-scale veins in the basalts display a “ladder” pattern, or an H-shaped abutment (Hancock, 1985), where the N–S veins are longest. In contrast, the deformation bands display a “grid” pattern with mutual crosscutting relationships (Rives et al., 1994). The orthogonal deformation bands are crosscut by shear deformation bands (Fig. 12c), suggesting an initial onset of extensional joints, followed by shear. Figure 12d and e shows the rose diagrams for the orthogonal patterns in the basalt and sandstone, respectively, in the Cerro do Jarau area.

5.2 Fracture patterns of NE–SW-directed paleostress field

The geometry of the fractures formed in the NE–SW-directed paleostress field shows an asymmetric distribution for the dextral and sinistral conjugated branches (Fig. 13). This asymmetric distribution of fracture orientation frequency allows them to be classified according to the Riedel shear criteria. However, the fault-slip data for the NE–SW paleostress field show that higher frequency Riedel fractures vary between sites, being classified as either R-type, C-type, P-type, or even hybrid fractures.

The rose diagrams for the NE–SW paleostress field are in accordance with field observations of fracture splaying. The R- and C-type fractures usually merge into one another to produce both dextral or sinistral splayed fractures and duplex strike-slip patterns. Such fracture patterns are the locus for mineralization. Fracture surfaces and open dilatational spaces are coated by celadonite ± chalcedony ± calcite. Hydraulic breccias are also recognized, but with minor frequency.

Some rose diagrams in Fig. 13 indicate the presence of extension to the hybrid joints (Hancock, 1985) and additionally, Fig. 13e and f suggests the development of the orthogonal fracture pattern in this second deformational phase. In the Cerro do Jarau giant intertrap dune (Fig. 7a), the N–S orthogonal deformation bands are also superposed by “grid” patterns of orthogonal NE–SW deformation bands (Fig. 14a). Careful measurement and evaluation of the orthogonal patterns at a number of outcrops permitted the construction of a rose diagram for this second generation of deformation

bands (Fig. 14b). The dispersion of the orthogonal NE–SW deformation bands also suggests the interplay of extensional and hybrid joints.

6 Analysis of the deformational phases

The deformational structures of the volcanic rocks of the Serra Geral Fm. were developed during the Jurassic to Cretaceous periods. Lava flow stratigraphy differs in each of the studied sites/areas (Heemann, 1997, 2005; Reginato, 2003; Acauan, 2007; Amorim, 2007), and it is still not possible to correlate the studied quarries to specified time intervals taking into account stratigraphic elements. However, the fault-slip investigations were constrained to the Serra Geral Fm. volcanics and intertrap sediments, which left the exact time of onset of the first deformational phase to be defined.

The paleostress analysis distinguished two different deformational phases in the Serra Geral Fm. volcanic rocks (Paraná Basin). The relative ages of the deformational events were established from field observations (Table 1), regional-scale folds (Fig. 5), and domes and basins (Fig. 7). The N–S-oriented stress field was assessed as being older than the NE–SW-oriented stress field deformational phase during the Jurassic to Cretaceous periods.

The regional-scale folds and the dome-and-basin features (Figs. 5 and 7) were shown to pertain to two distinct groups: (i) those with N–S and E–W elongations and (ii) those with NE and NW elongations. These directions are closely related to that determined for the orthogonal fracture patterns and faults in the previous sections. Considering Figs. 5, 7–10, 12, and 13, it can be established that a relationship of symmetry exists between the fractures, faults, and folds of the elongated domes and basins. Thus, the association between buckling processes and brittle deformation will be further analyzed to define their relationships and role in each deformational phase.

The presence of gentle domes and basins with their longest axes oriented in orthogonal directions suggests a regime of bi-directional compression ($\sigma1 \sim \sigma2 > \sigma3$). Gosh and Ramberg (1968) and Gosh et al. (1995) performed experimental investiga-

tions into the development of domes and basins under constrictional deformation. The Serra Geral Fm. field data do agree with experimental results in that: (i) domes and basins are elongated in orthogonal directions (Fig. 7a), (ii) domes and basins of the same deformational phase do not interfere with each other, but merge or abut without crossing (Fig. 7a), and (iii) the orthogonal fracture patterns and deformation bands are set parallel and perpendicular to the elongated fold hinge (Fig. 15).

A constrictional deformation regime is usually characterized by a stress difference ratio close to 1 ($D = \Phi \sim 1$). It is common practice to evaluate the stress state from the stress ratio ($D = \Phi$; Angelier, 1989) and Fig. 16a shows a histogram based on the results of the linear inversion method (Gauss method; Žalohar and Vrabec, 2007). It can be seen that the D ratio shows a wide dispersion for the first deformational phase, varying from 0.8 (area C), to 0.–0.3 in most of the studied sites.

The stress state for each deformational phase can also be evaluated on the diagram proposed by Lisle (1979). This diagram (Fig. 16b) shows that the stress tensors for each site/area are distributed in a linear pattern. This pattern suggests that the main stress difference ($\sigma1–\sigma3$) remains approximately constant, while $\sigma2$ encompasses most of the variation. The N–S-oriented stress field varies from a multidirectional stress field ($\sigma1 > \sigma2 \gg \sigma3$), towards a field where the major stress tensor is greater than the other two ($\sigma1 \gg \sigma2 \geq \sigma3$). The NE–SW-oriented stress field, however, is constrained to the field where the major compressive tensor is greater than the other two.

The Morris and Ferril (2009) diagram analyzes the slip tendency of rock mass discontinuities in terms of effective stress; i.e., the diagram can distinguish the influence of fluid pressure (Fig. 16c). The first deformational phase (N–S paleostress) plots in two separate parallel lines of constant slip tendency (Ts = 1.3 and 1.5). These two parallel lines suggest the varying influence of the intermediate stress tensor (σ_2) on the deformation. However, the second deformational phase (NE–SW paleostress) data correlate with a linear equation whose angular coefficient is > -1.0, which shows the influence of variations of both the σ_1 and σ_2 tensors on the deformation.

The fault-slip data inversion also allows the strain condition of the deformational phases to be evaluated (e.g., Marrett and Allmendinger, 1990; Cladouhos and Allmendinger, 1993; Žalohar and Vrabec, 2008). Figure 17 shows the logarithmic diagram for strain ratio derived from the Gauss Method (Žalohar and Vrabec, 2007), and from the MSM (Žalohar and Vrabec, 2008). The MSM allows the strain ratio to be determined from the total displacement gradient tensor of all measured fault sets, weighted by the number of faults in each set, number of fault sets (their symmetry), and resolved shear stress (Žalohar and Vrabec, 2008). The MSM strain values were defined by varying slightly the coefficient of residual friction (φ_2) in the T-Tecto program. Such a procedure brought closer adjustment of the stress (Gauss) and strain (MSM) tensors, because the axis of rotation is closer to a main tensor. Tables 5 and 6 show that the coefficients of residual friction (φ_2) determined from both the Gauss and MSM inversion techniques are largely similar. The greatest difference in friction coefficient (7–10°) is related to those sites/areas with a small number of fault-slip data, or asymmetric fault-slip sets.

Figure 17a represents the strain derived from the linear inversion technique and shows that deformation was developed under constrictional conditions. This result is consistent with the remote stress field, as discussed above. However, the strain ratio determined from the MSM shows that both deformational phases could be distinguished based on this parameter, but follow a flattening strain path (Fig. 17b). This flattening strain path results from a local stress field, because most of the investigated sites represent a single outcrop. However, it must be noted that the flattening strain path (Fig. 17b) is consistent in the volcanic rocks of the Paraná Basin, even for sites combining two or more outcrops (see Žalohar and Vrabec, 2008). The highest (ε_2–ε_3) MSM strain ratio is achieved in those sites where conjugated faults or symmetric fault sets are best developed (see Fig. 13). Additionally, the flattening strain path is best developed for the second deformational phase, which could be a consequence of the higher degree of fractures inherited from the original basalt flows and the first deformational phase.

The strain–ratio diagrams indicate a bi-directional constrictional deformation of the Paraná Basin for both phases. However, a deformational model must be developed to account both for the remote and local stress/strain fields and for the observed fracture patterns.

The deformational structures under investigation were developed upon the basalts to dacites of the Serra Geral Fm. (Paraná Basin). The volcanic flows show large lateral extensions and are usually thick (> 20 m); the main part of the basaltic flows are dominantly massive (Heemann, 1997, 2005; Reginato, 2003; Acauan, 2007; Amorim, 2007). Thus, the buckling deformation must have been produced by a tangential longitudinal mechanism (Ramsay, 1967, p. 391–415) and the neutral surface must have played an important role in local strain partitioning and the development of the structures. Figure 18, based on the discussion by Lisle (1999), summarizes a geometric model relating constrictional domes and basins, orthogonal fracture patterns, deformation bands, and conjugated faults.

The relations of symmetry of joints and faults to folds have long been investigated (e.g., Stearns, 1978; Hancock, 1985; Cosgrove and Ameen, 1999). The geometry of the domes and basins in the Paraná Basin volcanics (Fig. 7) has to consider bi-directional constriction in which both the major and intermediate ($\sigma_1 \geq \sigma_2$) remote tensors are horizontal. The buckling mechanism operating simultaneously in the orthogonal direction gave rise to a local flattening strain field in the outer part of the single flows, and open orthogonal extensional joints (Fig. 18). The fault-slip data, orthogonal joints, veins, and deformation bands were measured at the outcrop scale and then developed to the outer buckled rim of each single volcanic flow of the Paraná Basin.

The elongation ratio of the domes and basins and their gentle interlimb angles do not suggest large departures between the orientations of the remote and local tensors. Thus, even though the magnitudes and spatial distributions of the remote and local tensors differ, the extensional joints closely parallel the main tensors and the axes of the domes and basins (cross bc and ac joints: Hancock, 1985). This deformational model

accounts for the square (Fig. 2f) or rectangular (Fig. 12a) symmetry of the orthogonal veins, and for the "grid-type" deformation bands (Figs. 12b and 14a).

The regional distribution of veins and dykes (Fig. 11) is in accordance with this deformation history for the Paraná Basin volcanics. The emplacement of the thermally metamorphosed sandstone dykes could be attributed to the mobilization of the still unconsolidated sands from the underlying Botucatu Fm., or from the Botucatu sands interlayered (intertrapped) between the sequences of lava flows, into orthogonal extensional joints opened in the outer rim of the buckled volcanic flows.

The shear fractures (hybrid joints and faults) display a conjugated arrangement with regard to the extensional joints (Figs. 10, 11 and 13), but they started to develop just after the orthogonal fractures. The symmetry of the hybrid joints and faults is related to hk0 patterns in acute or obtuse angles to the elongated fold axis (Hancock, 1985).

The strike-slip stress field determined from the fault-slip data (Sects. 4 and 5) for both the first and second deformational phases appears to be inconsistent with the local flattening strain field in the outer part of the buckled volcanic flows. The fault-slip data showed that rather than the major compressive tensor being vertical, it was the local intermediate compressive tensor (σ_2) instead. However, the onset extensional joints induce local stress release in the σ_1 direction and a permutation between the local σ_1 and σ_2 tensors. The local stress release generates strike-slip faults (hk0 fault symmetry pattern). These deformational conditions explain the connection of extensional joints and hybrid to shear fractures, as shown in Figs. 2 and 11A.

The extensional joints and their splays to hybrid and shear fractures frequently have hydraulic breccia (Fig. 2). Such a feature points to supra-hydrostatic conditions ($P_f/P_{grav} > 0.5$) during the deformation, which favor the development of extensional joints. Veins and associated hydraulic breccia are also developed on fractures related to the second deformational phase, i.e., the supra-hydrostatic conditions remained active during this deformational phase.

This structural model of the constrictional deformation in the Paraná Basin also accounts for other important features observed in the volcanic flows. Small-scale folds,

similar to that in Fig. 7e, are recorded on basal horizontally jointed portions of the volcanic flows (Fig. 19). These small-scale folds are frequently truncated by fracture zones at their limbs. These folds are developed in the inner zone of the dome-and-basin structures, which is the locus for the local constrictional stress/strain in the tangential–longitudinal mechanism (Fig. 19c). Thus, it can be concluded that buckling of a single lava flow gave rise to the distinguishing deformational structures on either side of its neutral surface. At the outer rims, orthogonal extensional joints developed and sandstones dykes were emplaced, while at the inner rims, non-cylindrical folds developed.

The bi-directional constrictional deformation in the Paraná Basin during the Jurassic to Cretaceous periods accounts for the outcrop-scale alternation of σ_3 position, i.e., either N–S or E–W in the first deformational phase, or NE or NW in the second deformational phase. In fact, the different σ_1 and σ_3 orientations distinguished in Figs. 8 and 9 are not related to local σ_1 and σ_2 permutations on the outer rims of the folded volcanic flows. It should be noted that σ_1 and σ_3 orientations alternate between different investigation sites. Thus, it can be concluded that σ_1 and σ_3 orientations, inverted from fault-slip data, are related to the elongation of the dome-and-basin structures developed in each area. The bi-directional constrictional ($\sigma_1 \geq \sigma_2 \gg \sigma_3$) stress regime gave rise to orthogonally oriented domes and basins, as shown by Gosh and Ramberg (1968) and Gosh et al. (1995), which controlled the local distribution of extensional joints and strike-slip faults.

7 Conclusions

The Gauss and MSM paleostress inversion methods (Žalohar and Vrabec, 2007, 2008) were applied to fault-slip data for 42 sites in the southeast border and central regions of the Paraná Basin (Brazil). A number of fieldwork campaigns were undertaken to map the important structural features of the Paraná Basin that developed during the Jurassic to Cretaceous periods.

The geometric and kinematic analyses of the field data permitted two deformational phases during the Jurassic to Cretaceous periods to be distinguished. The paleostress-inversion-based distinction of fracture orientation families introduces biased results in some previous papers. The field-based data (fault-slips, fracture patterns, dykes, and contact attitudes) and data derived from paleostress inversions and kinematic analyses are in agreement with each of the deformational phases.

Both deformational phases developed under regional bi-directional constrictional ($\sigma_1 \geq \sigma_2 \gg \sigma_3$) stress regimes and gave rise to a number of non-cylindrical folds. These structures are characterized as domes and basins, and regional anticlines and synclines. Consequently, both deformational phases produced similar local-scale structures. However, these deformational phases can be distinguished both by the orientation of their structures and by some other structural features. The first deformational phase shows elongated domes and basins oriented both N–S and E–W. The second deformational phase also shows elongated domes and basins, but these are oriented NW–SE and NE–SW, according to the most expressive Ponta Grossa and Rio Grande arcs, and the Torres Syncline in the eastern border region of the Paraná Basin. These conditions indicate a clockwise rotation (35–40°) for both horizontal principal stress tensors ($\sigma_1 \geq \sigma_2$) during the Cretaceous period.

The paleostress orientation derived from fault-slip data, however, is related to the local stress field developed upon the buckled single volcanic flows of the Serra Geral Fm. The orthogonal patterns of the dykes and veins retain symmetric relationships with the fold axes of the elongated domes and basins. These orthogonal extensional joints are developed in the outer rims of the folded volcanic flows; however, the strike-slip faults follow the development of extensional joints. The strike-slip faults are the result of the stress drop after the onset of the extensional joints, which enabled a local permutation between σ_1 and σ_2. The hk0 symmetry for the strike-slip faults in the arcuate folds is in accordance with field observations.

The inner rims of the buckled volcanic flows, however, developed local arcuate folds, whose local stress axes are close to the regional ones. It should be noted that local-

scale folds could reproduce the regional bi-directional constrictional regime. Further investigations are needed to address this point in the future.

The outcrop-scale alternation of the σ_3 position, either N–S or E–W (D1 phase), or NE or NW (D2 phase), is not related to stress drop. The different σ_1 and σ_3 orientations distinguished in Figs. 8 and 9 are mainly reported in different investigation sites and result from the orientation of the arcuate fold minor axis. The σ_3 position depends on the orientation of the orthogonal elongated domes and basins. Thus, further investigation is in progress to determine the regional (remote), rather than local stress/strain field in the Jurassic to Cretaceous periods of the Paraná Basin.

Author contributions. A. J. Strieder, R. Heemann, P. A. R. Reginato, R. B. Acauan, V. A. de Amorim, and M. Z.Remde participated in the study design and concept, data collection, and data analysis and interpretation during the first stages of the investigation. A. J. Strieder also supervised all the investigation and conducted the second stage of field work, data analysis and interpretation. A. J. Strieder wrote the main manuscript, and R. Heemann, P. A. R. Reginato, R. B. Acauan, V. A. de Amorim, and M. Z. Remde conducted critical review and suggested amendments to the final manuscript.

Acknowledgements. The authors especially thank Jure Žalohar for kindly providing a license for the T-Tecto 3.0 software (http://www2.arnes.si/~jzaloh/t-tecto_homepage.htm), and for reading the article and offering comments and suggestions for its improvement. The authors also thank Luis Eduardo S.M. Novaes and Bardo Bodmann for their comments regarding this work.

We also extend our gratitude to the reviewers for their careful consideration and comments that have helped us improve the quality of the article.

The authors thank the Brazilian research agencies (FAPERGS, CNPq, CAPES, FINEP) for supporting the initial projects regarding the Paraná Basin volcanic rocks, and the Universidade Federal de Pelotas for supporting and encouraging the more recent local and regional fieldwork campaigns.

References

Aboy, M. and Masquellin, H.: Relações embasamento vs. cobertura na Ilha Cristalina de Rivera, Uruguai, in: Simpósio Sul-brasileiro de Geologia, Abstracts, SBG, Porto Alegre (Brazil), 126, 2013.

Acauan, R. B.: Geologia e controle estrutural das ocorrências de ágatas e ametistas na região de Quaraí/Santana do Livramento (RS), M.S. thesis, PrPG em Engenharia de Minas, Metalurgia e Materiais, UFRGS, Brazil, 167 pp., 2007.

Almeida, F. F. M.: Síntese sobre a tectônica da Bacia do Paraná, in: Simp. Regional de Geologia, 3, SBG-SP, Curitiba (Brazil), 1, 1–20, 1981.

Amorim, V. A.: Modelagem geológica e controle dos depósitos em geodos no Distrito Mineiro de Ametista do Sul (RS, Brasil), M.S. thesis, PrPG em Engenharia de Minas, Metalurgia e Materiais, UFRGS, Brazil, 173 pp., 2007.

Angelier, J.: From orientation to magnitudes in paleostress determinations using fault slip data, J. Struct. Geol., 11, 37–50, 1989.

Angelier, A. and Mechler, P.: Sur une méthode graphique de recherche de constraintes principales également utilisable et en séismologie: la méthode des diédres droits, Bull. Soc. Geol. Fr., 19, 1309–1318, 1977.

Artur, P. C. and Soares, P. C.: Paleoestruturas e petróleo na bacia do Paraná, Brasil, Revista Brasileira de Geociências, 32, 433–448, 2002.

Bai, T., Maerten, L., Gross, M. R., and Aydin, A.: Orthogonal cross joints: do they imply a regional stress rotation?, J. Struct. Geol., 24, 77–88, 2002.

Caputo, R.: Evolution of orthogonal sets of coeval extension joints, Terra Nova, 7, 479–490, 1995.

Caputo, R. and Hancock, P. L.: Crack-jump mechanism and its implications for stress cyclicity during extension fracturing, J. Geodyn., 16, 34–59, 1999.

Chang, H. K., Kowsmann, R. O., Figueiredo, A. M. F., and Bender, A. A.: Tectonics and stratigraphy of the East Brazil rift system: an overview, Tectonophysics, 213, 97–138, 1992.

Cladouhos, T. T. and Allmendinger, R. W.: Finite strain and rotation from fault-slip data, J. Struct. Geol., 15, 771–784, 1993.

Cosgrove, J. W. and Ameen, M. S.: A comparison of the geometry, spatial organization and fracture patterns associated with forced folds and buckled folds, Geol. Soc. Spec. Publ., 169, 7–22, 1999.

Ferreira, F. J. F.: Integração de Dados Geofísicos e Geológicos: Configuração e Evolução Tectônica do Arco de Ponta Grossa. Dissertação de Mestrado, PPG em Geoquímica e Geotectônica, IG-USP, São Paulo (Brasil), 273 pp., 1982.

Ferreira, F. J. F., Monma, R., Campanha, G. A. C., and Galli, V. L.: Na estimate of the degree of crustal extension and thinning associated with the Guapiara Lineament based on aeromagnetic modelling, Boletim IG-USP, Série Científica, 20, 69–70, 1989.

Gosh, S. K. and Ramberg, H.: Buckling experiments on intersecting fold patterns, Tectonophysics, 5, 89–105, 1968.

Gosh, S. K., Khan, D., and Sengupta, S.: Interfering folds in constrictional deformation, J. Struct. Geol., 17, 1361–1373, 1995.

Hancock, P. L.: Brittle microtectonics: principles and practice, J. Struct. Geol., 7, 437–457, 1985.

Heemann, R.: Geologia, controles e guias prospectivos dos depósitos de ágata na região de Salto do Jacuí (RS), M.S. thesis, PrPG em Engenharia de Minas, Metalurgia e Materiais, UFRGS, Brazil, 107 pp., 1997.

Heemann, R.: Modelagem exploratória estrutural e tridimensional para a prospecção dos depósitos de ágata do Distrito Mineiro de Salto do Jacuí (RS), Ph.D. thesis, PrPG em Engenharia de Minas, Metalurgia e Materiais, UFRGS, Brazil, 163 pp., 2005.

Jacques, P. D., Machado, R., Oliveira, R. G., Ferreira, F. J. F., Castro, L. G., and Nummer, A. R.: Correlation of lineaments (magnetic and topographic) and Phanerozoic brittle structures with Precambrian shear zones from the basement of the Paraná Basin, Santa Catarina State, Brazil, Bra. J. Geol., 44, 39–54, 2014.

Jaeger, J. C.: Elasticity, Fracture and Flow: With Engineering and Geological Applications, Chapman & Hall, London, 268 pp., 1969.

Leinz, V., Bartorelli, A., and Isotta, C. A. L.: Contribuição ao estudo do magmatismo basáltico Mesozóico da Bacia do Paraná, Academia Brasiliera de Ciências, 40, 167–181, 1968.

Lisboa, N. A. and Schuck, M. T. G. O.: Identificação de padrões estruturais no Grupo São Bento, Quarai, RS, através de imagens orbitais e sub-orbitais, Pesquisas em Geociências, 20, 5–23, 1987.

Lisle, R. J.: The representation and calculation of the deviatoric component of the geological stress tensor, J. Struct. Geol., 1, 317–321, 1979.

Lisle, R. J.: Predicting patterns of strain from three-dimensional fold geometries: neutral surface folds and forced folds, Geol. Soc. Spec. Publ., 169, 213–221, 1999.

Machado, R., Roldan, L. F., Jacques, P. D., Fassbinder, E., and Nummer, A. R.: Tectônica transcorrente Mesozoica-cenozóica no Domo de Lages – Santa Catarina, Revista Brasileira de Geociências, 42, 799–811, 2012.
Marrett, R. and Allmendinger, R. W.: Kinematic analysis of fault-slip data, J. Struct. Geol., 12, 973–986, 1990.
Marshak, S. and Mitra, G.: Basic Methods of Structural Geology, Prentice Hall, New Jersey (USA), 446 pp., 1988.
Meirelles, M. C.: Determinação da resistência ao cisalhamento de enrocamentos da UHE Machadinho através de ensaios de cisalhamento direto de grandes dimensões, M.S. thesis, PrPG Engenharia Civil, UFSC, Brazil, 123 pp., 2008.
Morgan, W. J.: Hotspot tracks and the early rifting of the Atlantic, Tectonophysics, 94, 123–139, 1983.
Morris, A. P. and Ferrill, D. A.: The importance of the effective intermediate principal stress (σ'_2) to fault slip patterns, J. Struct. Geol., 31, 950–959, 2009.
Northfleet, A. A., Medeiros, R. A., and Mühlmann, H.: Reavaliação dos dados geológicos da Bacia do Paraná, Boletim Técnico da Petrobras, Rio de Janeiro, 12, 291–346, 1969.
Nummer, A. R., Machado, R., and Jacques, P. D.: Tectônica transcorrente mesozoica/cenozoica na porção leste do Planalto do Rio Grande do Sul, Brasil, Pesquisas em Geociências, 41, 121–130, 2014.
Petit, J. P.: Criteria for the sense of movement on fault surfaces in brittle rocks, J. Struct. Geol., 9, 597–608, 1987.
Quintas, M. C. L.: O embasamento da Bacia do Paraná: reconstrução geofísica de seu arcabouço, Tese de Doutoramento, PPG em Geofísica (IAG-USP), São Paulo (SP), 213 pp., 1995.
Ramsay, J.: Folding and Fracturing of Rocks, McGraw-Hill, New York, 568 pp., 1967.
Reginato, P. A. R.: Integração de dados geológicos para prospecção de aquíferos fraturados em trecho da Bacia Hidrográfica Taquari-Antas (RS), Ph.D. thesis, PrPG em Engenharia de Minas, Metalurgia e Materiais, UFRGS, Brazil, 286 pp., 2003
Reginato, P. A. R. and Strieder, A. J.: Caracterização estrutural dos aquíferos fraturados da Formação Serra Geral na região nordeste do Estado do Rio Grande do Sul, Revista Brasileira de Geociências, 36, 13–22, 2006.
Remde, M. Z.: A megaduna intertrap do Cerro do Jarau (RS), B.S. thesis, Engenharia Geológica, CDTec-UFPel„ 95 pp., 2013.

Riccomini, C.: Tectonismo gerador e deformador dos depósitos sedimentares pós-gondvânicos da porção centro-oriental do Estado de São Paulo e áreas vizinhas, Tese de Livre Docência, Instituto de Geociências, Universidade de São Paulo, São Paulo (Brasil), 100 pp., 1995.
Rives, T., Rawnsley, K. D., and Petit, J. P.: Analogue simulation of natural orthogonal joint set formation in brittle varnish, J. Struct. Geol., 16, 419–429, 1994.
Rostirolla, S. P., Assine, M. L., Fernandes, L. A., and Artur, P. C.: Reativação de Paleolineamentos durante a evolução da Bacia do Paraná – O Exemplo do Domo de Quatiguá, Revista Brasileira de Geociências, 30, 639–648, 2000.
Scherer, C. M. S. and Lavina, E. L. C.: Stratigraphic evolution of fluvial-eolian sucession: the example of the Upper Jurassic–Lower Cretaceous Guará and Botucatu formations, Paraná Basin, Southern Brazil, Gondwana Res., 9, 475–484, 2006.
Schobbenhaus, C. and Bellizzia, A.: Geological Map of South America, 1 : 500 000, CGMW – CPRM – DNPM – UNESCO, Brasília (Brazil), 2001.
Schuck, M. T. G. O. and Lisboa, N. A.: Caracterização de formas e padrões estruturais no Grupo São Bento da Bacia do Paraná no Rio Grande do Sul em imagens orbitais e suborbitais, in: Simpósio Brasileiro de Sensoriamento Remoto, 1988, Natal (Brazil), Anais, 2, 323–333, 1988.
Soares, A. P., Barcellos, P. E., Csordas, S. M., Mattos, J. T., Balieiro, M. G., and Meneses, P. R. Lineamentos em imagens de Landsat e Radar e suas implicações no conhecimento tectônico da Bacia do Paraná, in: Simp. Bras. Sens. Remoto, 2, Brasília, 143–168, 1982.
Soares, A. P., Soares, P. C., and Holz, M.: Correlações conflitantes no limite Permo-Triássico no sul da Bacia do Paraná: o contato entre duas superseqüências e implicações na configuração espacial do Aqüífero Guarani, Pesquisas em Geociências, 35, 115–133, 2008a.
Soares, A. P., Soares, P. C., and Holz, M.: Heterogeneidades hidroestratigráficas no Sistema Aqüífero Guarani, Revista Brasileira de Geociências, 38, 598–617, 2008b.
Stearns, D. W.: Faulting and forced folding in the Rocky Mountain foreland, Geol. Soc. Am. Mem., 151, 1–38, 1978.
Strieder, A. J. and Heemann, R.: Análise geométrica de estruturas de sucessão vulcânica associada aos depósitos de Ágata do Distrito Mineiro do Salto do Jacuí (RS), in: Simpósio Nacional de Estudos Tectônicos, Extended Abstracts, 1, Lençóis (BA), 14–16, 1999.
Strugale, M., Rostirolla, S. P., Mancini, F., Portela Filho, C. V., Ferreira, F. J. F., and Freitas, R. C.: Structural framework and Mesozoic–Cenozoic evolution of Ponta Grossa Arch, Paraná Basin, southern Brazil, J. S. Am. Earth Sci., 24, 203–227, 2007.

Tchalenko, J. S.: Similarities between shear zones of different magnitudes, Geol. Soc. Am. Bull., 81, 1625–1640, 1970.
Tchalenko, J. S. and Ambraseys, N. N.: Structural analysis of the Dasht-e Bayaz (Iran) earthquake fractures, Bull. Geol. Soc. Am., 81, 41–60, 1970.
Wilson, M.: Igneous Petrogenesis: a Global Tectonic Approach, Chapman & Hall Ed., London (UK), 466 pp., 1989
Zalán, P. V.: Evolução Fanerozóica das bacias sedimentares brasileiras, in: A Geologia do Continente Sul-americano, edited by: Neto, V. M., Bartorelli, A., Carneiro, C. D. R., and Brito-Neves, B. B., Editora Beca, São Paulo (Brazil), 595–613, 2004.
Zalán, P. V., Wolff, S., Astolfi, M. A. M., Vieira, I. S., Conceição, J. C. J., Appi, V. T., Neto, E. V. S., Cerqueira, J. R., and Marques, A.: The Paraná Basin, Brazil, AAPG Memoir., 51, 681–707, 1991.
Žalohar, J. and Vrabec, M.: Paleostress analysis of heterogeneous fault-slip data: the Gauss method, J. Struct. Geol., 29, 1798–1810, 2007.
Žalohar, J. and Vrabec, M.: Combined kinematic and paleostress analysis of fault-slip data: the multiple-slip method, J. Struct. Geol., 30, 1603–1613, 2008.
Zerfass, H., Chemale Jr., F., and Lavina, E. L. C.: Tectonic control of the Triassic Santa Maria Supersequence of the Paraná Basin, Southernmost Brazil, and its correlation to the Waterberg Basin, Namibia, Gondwana Res., 8, 163–176, 2005.

Table 1. Deformational phases distinguished in the uppermost units of the Paraná and in the continental rift basins of Southeast Brazil (Riccomini, 1995).

Def Phase	Time interval	Main geological features	Interpretation
D_n	Permian to Lower Cretaceous	Deformational event previous to Gondwana rupture NE-oriented basalt and clastic dikes Geophysical alignments	NW-oriented minimum stress (σ_3) axis
D_{n+1}	Upper Cretaceous	NW-oriented basalt dikes in the Ponta Grossa Arc region Final stages of the Serra Geral volcanism Jacupiranga Alkaline Intrusion Anticlinal dome structures	*NE basalt dikes and NW Ponta Grossa dikes were indicated to represent a triple junction remnant* NE-oriented minimum stress (σ_3) axis **Dextral transcurrent system**
D_{n+2}	Paleocene to Eocene	Bauru Basin structural development Rift (graben) basins at the continental margin NE-oriented lamprofiric dikes	NW-oriented minimum stress (σ_3) axis **Sinistral transcurrent system**
D_{n+3}	Eocene to Oligocene	Jaboticabal Alkaline Intrusion Hydrothermal sillicification contemporaneous to sedimentation of Itaqueri Fm.	NNW-oriented maximum stress (σ_1) axis **Dextral transcurrent system**
D_{n+4}	Miocene	Ultrabasic flows in Volta Redonda and Itaboraí Deposition of Itaquaquecetuba Fm. **Sinistral EW transcurrent system**	Maximum stress (σ_1) axis alternating from NS and EW according the balance between South Atlantic drifting and Nazca Plate subduction
D_{n+5}	Pliocene	**Dextral EW transcurrent system**	
D_{n+6}	Pleistocene to Holocene	NS-oriented grabens Extensional WNW–ESE regime	

Table 2. Paleostress fields defined by Heemann (1997, 2005), Reginato (2003), Acauan (2007) and Amorim (2007) for fault slip data of Serra Geral Fm using the method of Angelier and Mechler (1977).

	(σ_1)	(σ_2)	(σ_3)
Heemann (1997, 2005), Heemann and Strieder (1999)			
Salto do Jacuí and Sobradinho region (RS)			
Estrela Velha – Arroio do Tigre área	20–341	35–100	08–219
Sobradinho to Ibarama área	11–321	67–182	02–095
Saltinho área	06–334	72–218	02–120
	12–151	50–044	34–260
Eng. Maia Filho Damp area	04–343	30–250	58–095
	46–357	22–110	13–209
Angico Quarry	36–349	05–255	52–157
Poço Grande Quarry	19–358	14–091	12–178
Zubi and Ralph Quarries	67–341	04–079	23–172
	62–313	15–073	06–165
Pedreira Funda Quarry	50–332	07–086	05–171
Reginato (2003), Reginato and Strieder (2006)			
Caxias do Sul and Veranópolis region (RS)			
Pedreira Guerra Quarry	10–074	80–256	03–346
CODECA Quarry	01–174	86–084	04–264
	03–263	88–092	02–357
Tega Outcrop and Road cut	15–073	72–270	04–165
Veranópolis roadcut	10–068	80–248	02–158
Acauan (2007)			
Santana do Livramento and Quaraí region (RS)			
Santa Rita Quarry	11–032	87–182	07–301
	08–133	80–272	07–042
Registro Quarry	09–116	80–270	04–026
Amorim (2007)			
Ametista do Sul and Frederico Westphalen region (RS)			
Ametista do Sul quarries	25–028	54–330	23–115
Frederico Westph to Caiçara area	13–110	68–327	17–204
	09–170	72–328	17–083
	20–205	60–334	21–114
Rodeio Bonito Quarry	09–147	70–355	18–241
	29–232	54–355	21–139
Alpestre Quarry	11–119	74–345	10–209

Table 3. Summary of crosscutting relations of different striations observed in the same fault plane.

Site	Relative age	Fault plane	Striae orientation	Sense of movement
Pedreira Quarai	1st	359/73	20/173	Sinistral
	2nd	359/73	14/006	Dextral
Pedreira SF Assis	1st	066/72	27/236	Dextral
	2nd	066/72	27/077	Sinistral
Pedreira Painel	1st	166/72	09/343	Dextral
	2nd	166/72	10/169	Dextral
	1st	034/74	13/039	Sinistral
	2nd	034/74	60/185	Normal

Table 4. Parameters for stress inversion using multiple-slip method (Žalohar and Vrabec, 2008).

Parameter	Value range
Dispersion (s)	20
Threshold (Δ)	40–50
Shear strength ($\phi 1$)	50–65
Angle of residual friction ($\phi 2$)	20–35
Stress parameter	40–50
Andersonian regime set	Yes

The shear strength and angle of internal friction data for volcanic rocks of Paraná Basin are from fresh rock test (Meirelles, 2008).

Table 5. Summary of principal stress axes in the N–S and E–W orientations computed for sites within the volcanic rocks of the Paraná Basin.

Site	SD of s	Linear inversion				MSM inversion			
		$\sigma_1\ \sigma_2\ \sigma_3$	Relative values of λ_i	D	ϕ_2	$\sigma_1\ \sigma_2\ \sigma_3$	Relative values of λ_i	D	ϕ_2
A Compilation from PR (Ped Registro) and PQ2 (Ped Quaraí 2)	13	02/260 84/009 06/170	0.56 : −0.24 : −0.330.99 : 0.19 : 0.10	0.10	25	01/264 87/011 03/174	0.73 : −0.03 : −0.70	0.47	20
B Pedreira SF Assis 2 (BR377)	20	02/273 72/176 18/003	0.58 : −0.24 : −0.340.99 : 0.16 : 0.07	0.10	25	12/275 78/104 02/006	0.71 : 0.03 : −0.73	0.53	25
C Compilation from sites Estr Velha, Sobradinho1, and Saltinho1A	14	02/174 84/283 06/084	0.24 : 0.12 : −0.360.78 : 0.63 : 0.06	0.80	35	08/174 78/305 09/082	0.71 : 0.03 : −0.74	0.53	20
D Compilation from sites Angico and Poço Grande	17	12/184 76/030 06/275	0.48 : −0.11 : −0.370.94 : 0.35 : 0.09	0.30	35	01/190 83/094 07/280	0.73 : −0.01 : −0.73	0.49	35
E Compilation from sites Sobradinho2, Saltinho2, Gar Zubi, and Pedra Funda	17	02/260 84/152 06/350	0.52 : −0.17 : −0.350.97 : 0.27 : 0.10	0.20	30	03/086 87/239 01/356	0.71 : 0.01 : −0.71	0.51	30
F Compilation from sites Gar Ametista, Pedr Fred Westph, and Caiçara2	20	02/187 72/283 18/096	0.57 : −0.29 : −0.290.99 : 0.13 : 0.13	0.00	20	06/187 83/342 03/097	0.73 : −0.03 : −0.71	0.47	20
G Compilation from sites Pedr Guerra, CODECA1, Aflor Tega, and Veranópolis	11	02/076 84/328 06/166	0.59 : −0.25 : −0.341.01 : 0.17 : 0.07	0.10	25	01/072 88/324 02/162	0.79 : −0.02 : −0.77	0.48	30
H Pedr CODECA1	9	13/184 76/030 06/275	0.50 : −0.12 : −0.380.95 : 0.33 : 0.07	0.30	40	02/001 82/105 08/270	0.73 : −0.04 : −0.69	0.46	33
I Pedreira Painel	10	13/002 76/208 06/094	0.52 : −0.17 : −0.350.97 : 0.27 : 0.10	0.20	25	03/008 87/198 01/098	0.72 : 0.01 : −0.72	0.51	39

Results for the linear and multiple-slip methods of inversion are calculated by the T-TECTO 3.0 program, according to Žalohar and Vrabec (2007, 2008).

Table 6. Summary of principal stress axis in the NE–SW orientation computed for sites within the volcanic rocks of the Paraná Basin.

Site	SD of s	Linear inversion		D	ϕ_2	MSM inversion		D	ϕ_2
		$\sigma_1\ \sigma_2\ \sigma_3$	Relative values of λ_i			$\sigma_1\ \sigma_2\ \sigma_3$	Relative values of λ_i		
A Compilation from Pedr Sta Rita 1 + BR293 + Pedr Quarai 1	13	02/027 84/135 06/297	0.62 : −0.27 : −0.361.06 : 0.17 : 0.08	0.10	25	02/036 87/165 03/306	0.97 : −0.03 : −0.94	0.48	30
B Pedreira Sta Rita 2	11	02/309 84/201 06/040	0.65 : −0.27 : −0.371.10 : 0.18 : 0.08	0.10	25	04/113 85/337 04/203	0.82 : 0.01 : −0.83	0.51	35
C Pedreiras BR290 + BR377	16	02/223 72/320 18/133	0.57 : −0.19 : −0.381.06 : 0.30 : 0.11	0.20	25	08/039 80/254 06/130	1.03 : −0.10 : −0.92	0.42	25
D Compilation from sites Barragem M Filho and Gar Ralph	12	02/236 84/127 06/326	0.51 : −0.12 : −0.401.01 : 0.38 : 0.10	0.30	33	07/242 83/058 00/152	0.88 : −0.01 : −0.87	0.49	33
E Pedreira Dacito	16	13/142 76/296 06/051	0.65 : −0.28 : −0.391.11 : 0.18 : 0.08	0.10	30	04/143 72/247 17/052	1.03 : −0.21 : −0.82	0.33	32
F Compilation from sites Pedreiras FrWestph1, Caiçara1, RodBon1, and Planalto-Alpestre	16	02/125 84/234 06/035	0.57 : −0.19 : −0.381.05 : 0.29 : 0.10	0.20	30	04/126 85/273 03/036	0.98 : −0.04 : −0.93	0.47	25
G Pedreria Rodeio Bonito 2	8	13/058 76/264 06/150	0.52 : −0.12 : −0.391.01 : 0.37 : 0.10	0.30	33	15/040 75/230 02/131	0.96 : 0.04 : −1.00	0.53	40
H Rota dos Canions (RS)	18	02/039 84/148 06/309	0.57 : −0.19 : −0.381.06 : 0.30 : 0.11	0.20	30	09/041 81/216 01/310	1.02 : −0.08 : −0.95	0.44	30
I Compilation from sites Pedreiras BJSerra and Painel2	10	12/212 76/057 06/303	0.52 : −0.12 : −0.391.01 : 0.37 : 0.10	0.30	35	06/213 84/057 02/303	0.91 : 0.04 : −0.95	0.53	35

Results for the linear and multiple-slip methods of inversion are calculated using the T-TECTO 3.0 program, according to Žalohar and Vrabec (2007, 2008).

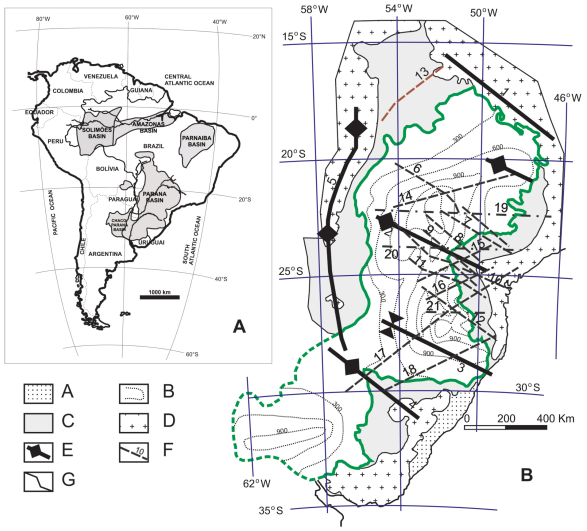

Figure 1. (a) Location of the Paleozoic–Mesozoic intracratonic basins of the South American continental plate (modified from Zalán et al., 1991); Chaco–Paraná Basin is actually covered by Tertiary and Quaternary sediments. **(b)** Geological sketch of the Paraná Basin and its main structural features (modified from Leinz et al., 1968; Zalán et al., 1991). Legend: (A) Quaternary sediments. (B) Serra Geral Fm.; dotted lines show the actual thicknesses of the volcanic rock piles. (C) Paleozoic to Mesozoic sedimentary rocks. (D) Basement rocks. (E) Structural highs, arches, and synclines. (F) Main fault zones (numbered): (1) Alto Parnaíba high, (2) Ponta Grossa Arc, (3) Torres Syncline, (4) Rio Grande Arc, (5) Asunción Arc, (6) Guapiara, (7) Santo Anastácio, (8) São Jerônimo–Criúva, (9) Rio Alonso, (10) Cândido de Abreu–Campo Mourão, (11) Rio Piquiri, (12) Caçador, (13) Transbrasiliano, (14) Araçatuba, (15) Guaxupé, (16) Jacutinga, (17) Lancinha–Cubatão, (18) Blumenau–Soledade, (19) Mogiguaçu–Dourados, (20) São Sebastião, (21) Taquara Verde. (G) Main rivers.

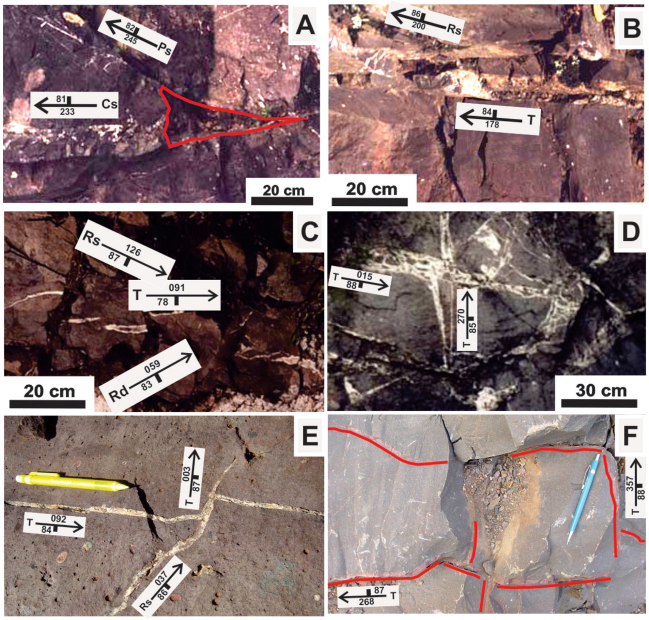

Figure 2. Fracture patterns in the Serra Geral Fm. volcanic rocks. **(a)** Fracture splay and a triangular zone showing hydraulic breccia (weathered). **(b)** Extensional joint terminating into R shear and hydraulic breccia. **(c)** Extensional joints terminating into either dextral or sinistral shear. **(d)** Different generation of extensional joints and hydraulic breccia. **(e)** Orthogonal extensional joints filled by thermally metamorphosed sandstone. **(f)** Orthogonal extensional joints filled by metamorphosed sandstone (the sandstone dykes were laterally delineated). R, C, and P are synthetic shear fractures; R′ indicates antithetic shear; T indicates extensional joints; s or d indicate sinistral or dextral fracture sense of movement, respectively. Notation for fracture orientation follows Fig. 3.

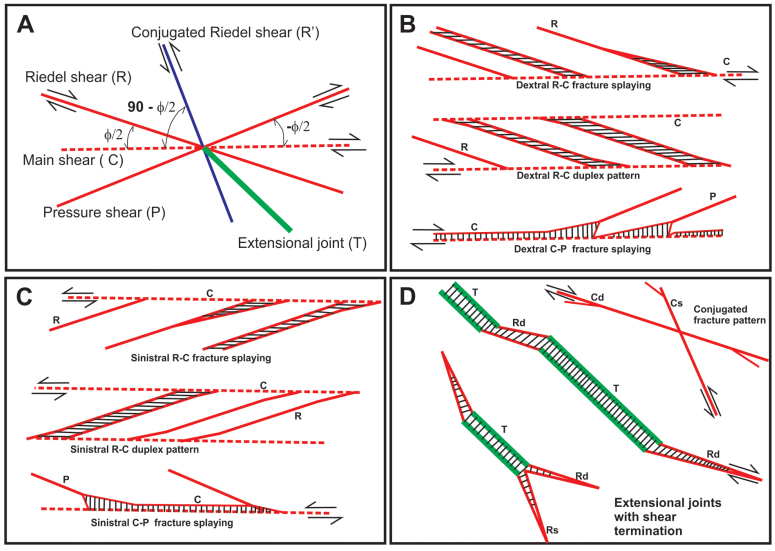

Figure 3. Field diagrams of fracture patterns in the volcanic rocks of the Serra Geral Fm. **(a)** Riedel-type fractures, as reported by Tchalenko (1970) and Tchalenco and Ambraseys (1970). **(b)** Dextral patterns of shear fractures. **(c)** Sinistral patterns of shear fractures. **(d)** Conjugated shear fractures and combinations of tension joints and shear fractures. Hatched areas represent transtensile dilatational spaces developed by shearing. R, C, and P are synthetic shear fractures; R' indicates antithetic shear; T indicates extensional joints; s or d indicate sinistral or dextral fracture sense of movement, respectively.

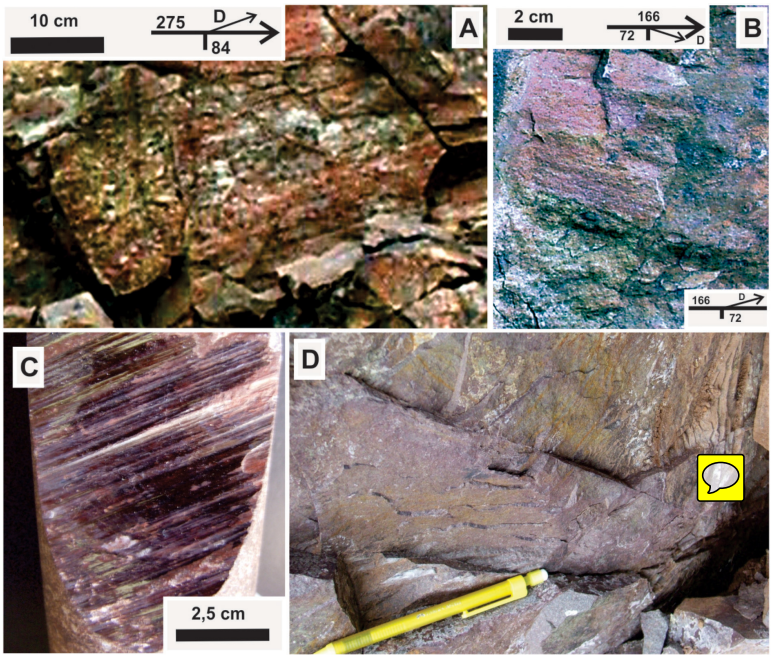

Figure 4. Geological features of the fault planes in the volcanic rocks of the Paraná Basin. **(a)** RM-type striation. **(b)** Overprinting of TM striation on former striation with mineralization in the same fault plane. **(c)** Frictional striae and steps in a polished fault plane. **(d)** Sub-centimeter fracture cleavage dragging the horizontal joints of basalt.

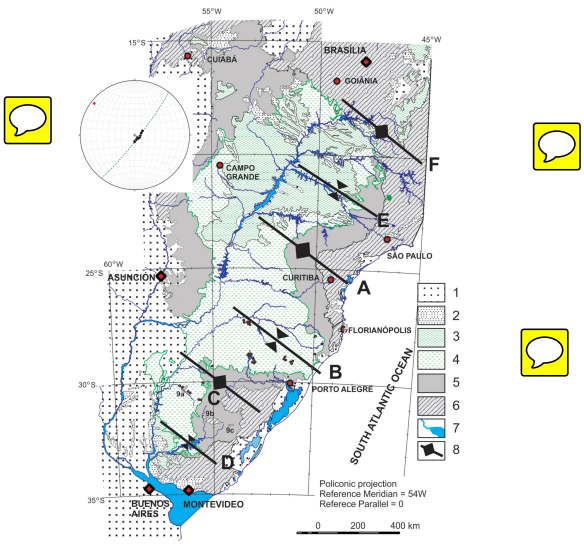

Figure 5. Regional folds developed by NE–SW paleostress tensors. (A) Map showing the location of synclines and anticlines (arcs), and also the domes and basins in the southern part of the Paraná Basin. (B) Lower hemisphere, equal area stereogram of the basal contact of the Serra Geral Fm. along the Rio Grande Arc and Torres Syncline. (1) Quaternary sediments. (2) Cenozoic sedimentary rocks. (3) Cretaceous to Paleogene sedimentary rocks. (4) Paraná Flood Basalts. (5) Paleozoic–Mesozoic sedimentary rocks of Paraná Basin. (6) Basement rocks. (7) Main rivers, lakes, and lagoons. (8) Main NW-oriented arcs and synclines. (9) Elongated domes: (a) Quaraí Dome, (b) Rivera Crystalline Island, (c) Aceguá Crystalline Island. Based on South America Geological Map (Schobbenhaus and Bellizzia, 2001). Small open dots represent outcrops where fault-slip data were measured and analyzed.

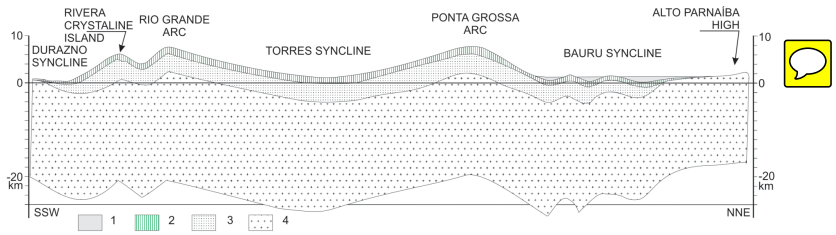

Figure 6. Balanced SW–NE cross section from Uruguay to São Paulo (Brazil) showing the gentle anticlines and synclines dipping NW in the eastern border of the Paraná Basin. The cross section is perpendicular to the fold hinge. (1) Cretaceous to Paleogene sedimentary cover. (2) Serra Geral Fm. (3) Paleozoic–Mesozoic sedimentary rocks of the Paraná Basin. (4) Basement. The structural section was built upon the South America Geological Map (Schobbenhaus and Bellizzia, 2001), and structural field data. The vertical exaggeration is 13×.

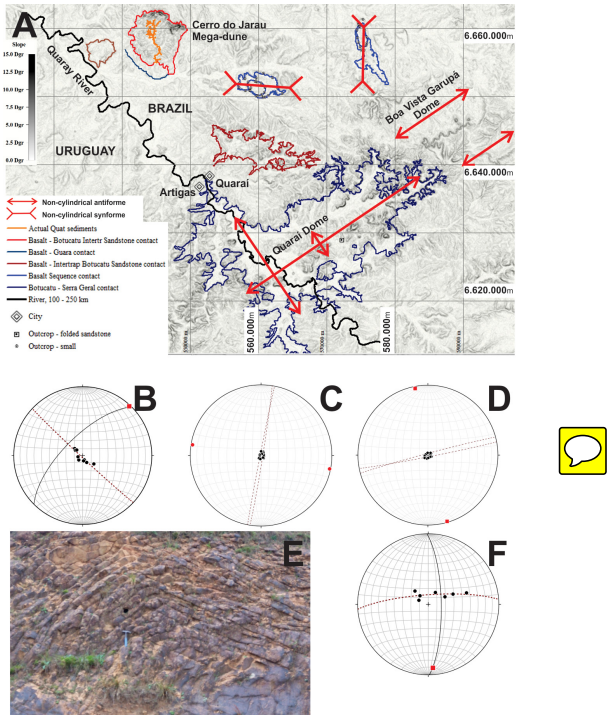

Figure 7. Dome and basin structures in the Quaraí Dome area. **(a)** Geological sketch indicating the main structural features in the region. **(b)** π diagram for sandstone–basalt contact in the Quaraí Dome. **(c)** π diagram for a basalt flow contact along the E–W basin. **(d)** π diagram for the basalt flow contact along the N–S basin. **(e)** South-dipping fold in Botucatu Fm. sandstone. **(f)** π diagram for sandstone in the road cut outcrop.

Discussion Paper | Discussion Paper | Discussion Paper | Discussion Paper |

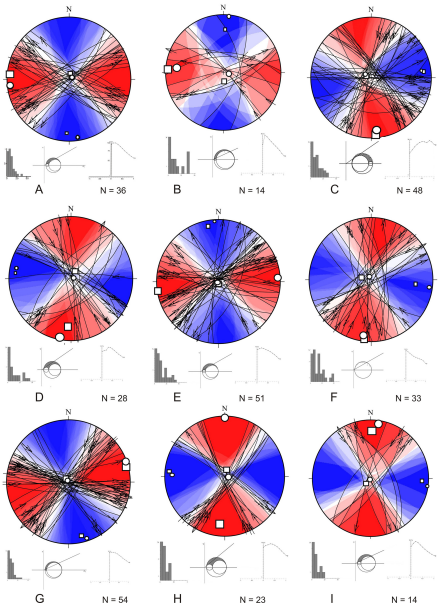

Figure 8. Paleostress results for the N–S and E–W tensors observed in the volcanic rocks of the Paraná Basin. Each area/site is identified by a capital letter. The graphics for each area/site include: lower hemisphere, equal area stereogram of brittle fault-slip data; misfit angle histogram; Mohr diagram for resolved shear stress; and biplot of the value for object function (M) vs. shape of the strain ellipsoid (D). Open circles and open squares in the stereograms represent stress direction determined using the Gauss and MSM methods, respectively. The sizes of the open circles and squares relate to the magnitudes of the stress tensors.

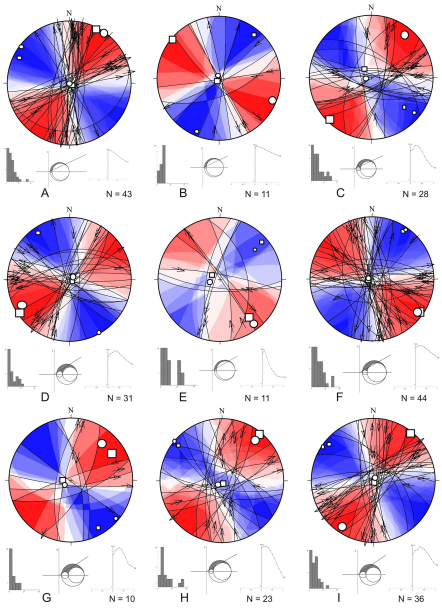

Figure 9. Paleostress results for NE–SW tensors observed in the volcanic rocks of the Paraná Basin. Each area/site is identified by a capital letter. The graphics for each area/site include: lower hemisphere, equal area stereogram of brittle fault-slip data; misfit angle histogram; Mohr diagram for resolved shear stress; biplot of value for object function (M) vs. shape of the strain ellipsoid (D). Open circles and open squares in the stereograms represent stress direction determined using the Gauss and MSM methods, respectively. The sizes of the open circles and squares relate to the magnitudes of the stress tensors.

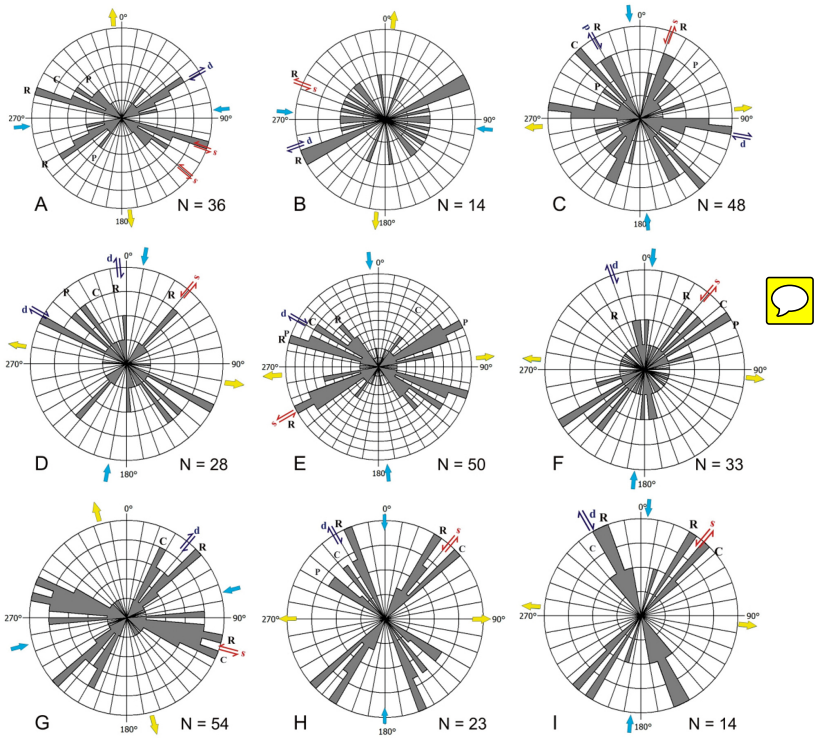

Figure 10. Rose diagrams of fault-slip data for N–S tensors. Circular histograms from **(a)** to **(i)** correspond to the sites/areas described in Table 3.

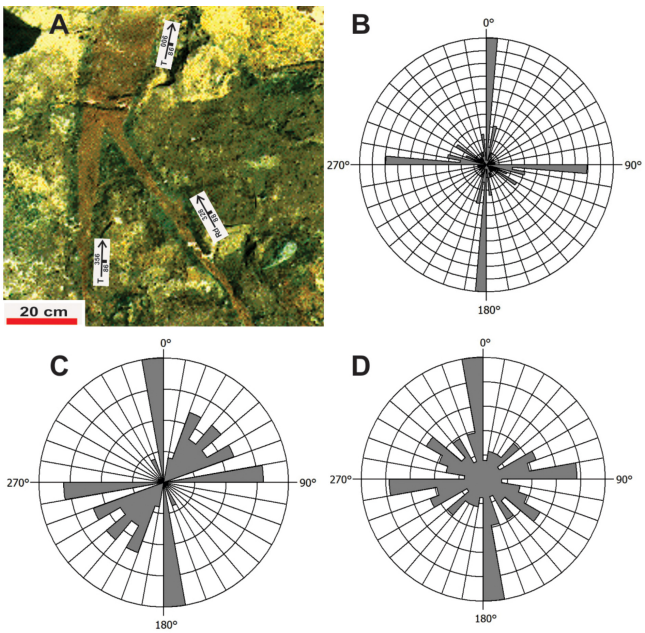

Figure 11. Tabular dykes emplaced into basalts of the Serra Geral Fm. **(a)** Photograph of the tabular dykes emplaced into the vesicular basalts of the Salto do Jacuí region. **(b)** Rose diagram of orientation of sandstone dykes in the Salto do Jacuí region (N = 135). **(c)** Rose diagram of orientation of sandstone dykes in the Caxias do Sul region (N = 24). **(d)** Rose diagram of orientation of mineralized veins in the Caxias do Sul region (N = 85).

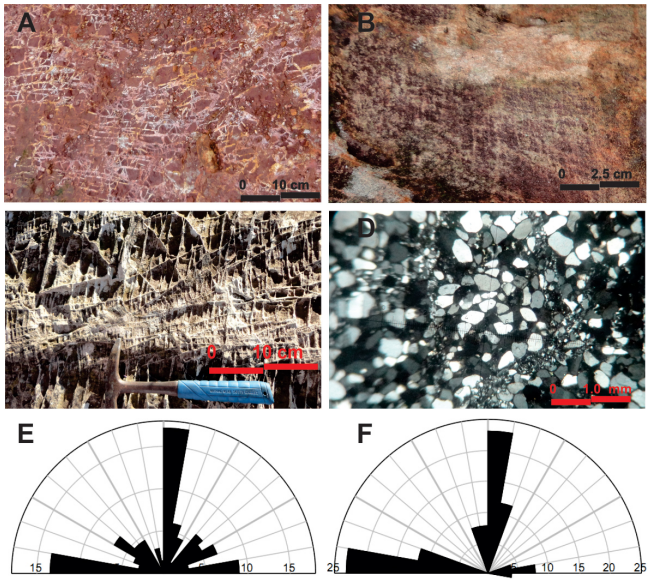

Figure 12. Orthogonal pattern features recorded in the Cerro do Jarau intertrap megadune. **(a)** Centimeter-scale orthogonal "ladder-type" veins in the basalt of the Cerro do Jarau hills. **(b)** Millimeter-scale orthogonal "grid-type" deformation bands in the Botucatu Fm. sandstone in the Cerro do Jarau intertrap dune. **(c)** Superposed shear deformation bands on orthogonal bands. **(d)** Thin section of thermally metamorphosed sandstone showing the orthogonal deformation bands. **(e)** Rose diagram of the orthogonal veins in basalts (N = 134). **(f)** Rose diagram of deformation bands in sandstones (N = 28).

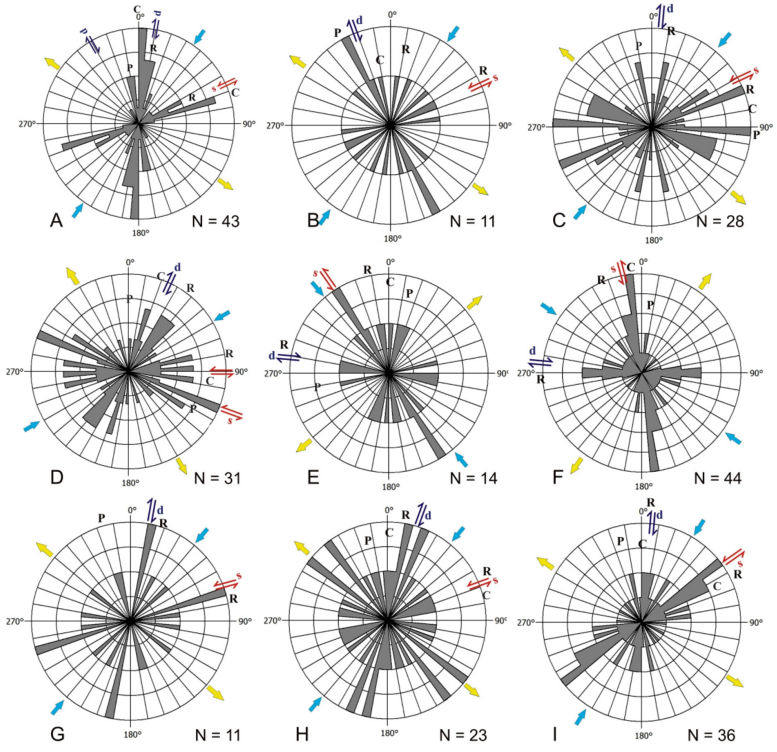

Figure 13. Rose diagrams of fault-slip data for NE–SW tensors. Circular histograms from **(a)** to **(i)** correspond to sites/areas described in Table 4.

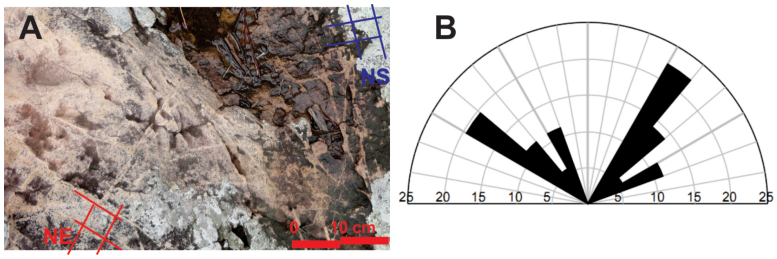

Figure 14. Orthogonal patterns associated with second deformational phase in the Cerro do Jarau area. **(a)** NE–SW orthogonal deformation bands superposed upon the N–S bands. **(b)** Rose diagram of the NE–SW orthogonal deformation bands (N = 36).

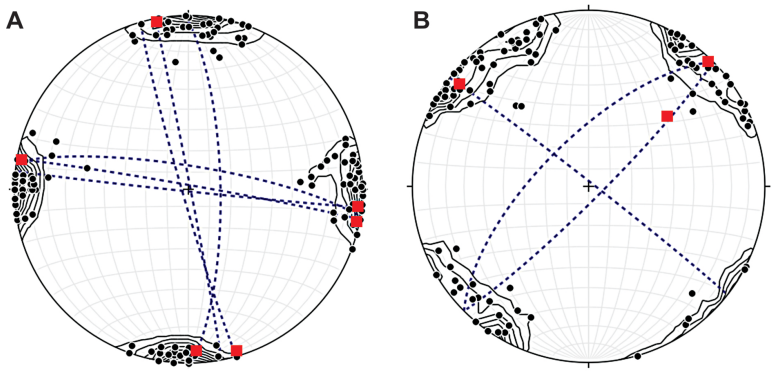

Figure 15. Lower hemisphere stereograms showing the symmetry relationships between domes and basins and fractures in the Paraná Basin volcanics. **(a)** Fold axis, extensional dykes and veins, and deformation bands of the first deformational phase in the Quaraí Dome area. **(b)** Fold axis for NW regional arcs, Quaraí Dome, extensional dykes and veins, and deformation bands of the second deformational phase. Dashed great circles are axial planes of folds and arcs.

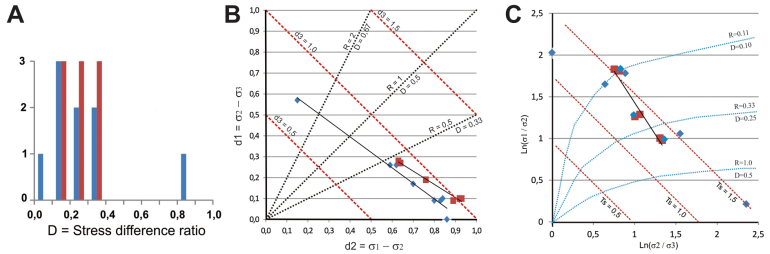

Figure 16. Diagrams for stress states of the deformation phases in the Serra Geral Fm. volcanics, as determined by the linear inversion technique. **(a)** Histogram for *D* values determined in each investigation area. **(b)** Stress differences diagram of Lisle (1979). **(c)** Stress ratio diagram of Morris and Ferrill (2009). Blue bars and diamonds represent N–S-oriented stress tensors. Red bars and squares represent NE–SW-oriented stress tensors. Thin black lines are the linear best fit for each paleostress regime. $R = d1/d2$ (Lisle, 1979). $D = \Phi$ (Angelier, 1989). $R = D/(1 - D)$.

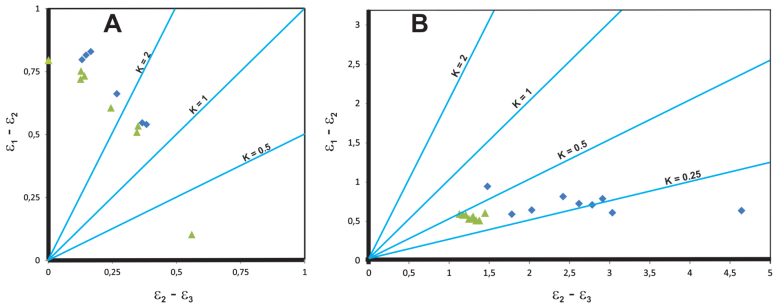

Figure 17. Strain-ratio log diagrams for volcanic rocks of the Paraná Basin. **(a)** Results from the linear inversion method (Žalohar and Vrabec, 2007). **(b)** Results from multiple-slip method (Žalohar and Vrabec, 2008). Green triangles represent the first deformational phase and blue diamonds the second.

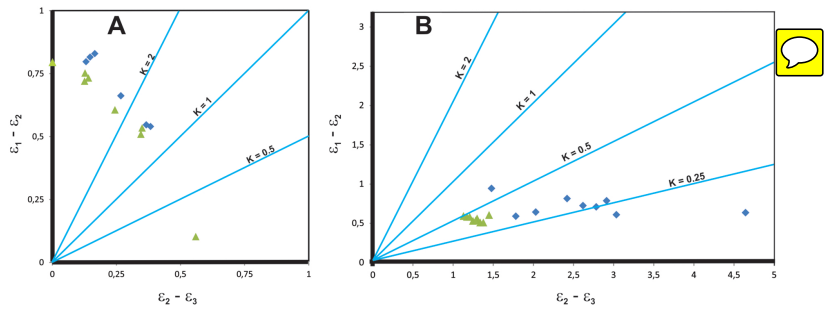

Figure 18. Bi-directional dome-and-basin model structures for the Serra Geral Fm. volcanics (Paraná Basin). **(a)** Regional sketch for orthogonal elliptical non-cylindrical folds. **(b)** Detail for local-scale stress/strain distribution in the tangential–longitudinal buckled volcanic layer; stippled line distinguishes the neutral surface. The principal curvature directions (contour lines for domes and basins) parallel to the principal strain directions give rise to orthogonal joints in the outer rims of non-cylindrical folds (Lisle, 1999).

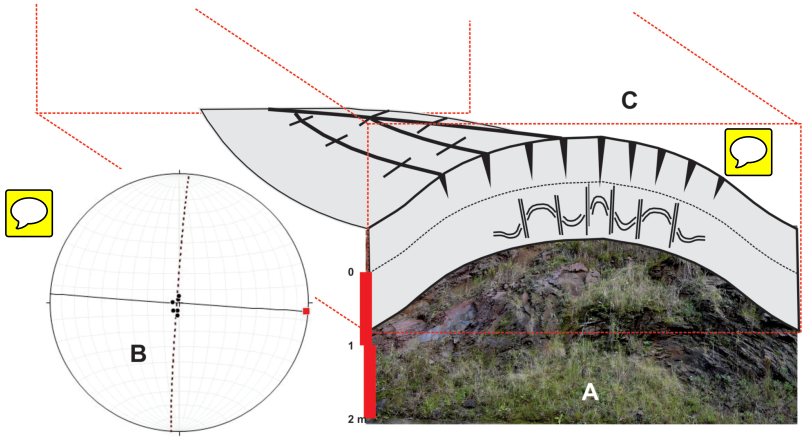

Figure 19. Small-scale fold on basal horizontally jointed basalt flow. **(a)** Outcrop-scale fold at base of a basalt flow. **(b)** Lower hemisphere stereogram for folded horizontal joints of the basalt flow. **(c)** Tangential–longitudinal buckle model distinguishing structural features developed at the outer and inner rims of a buckled single layer flow.